energies

MDPI

Article

Characteristics and Key Controlling Factors of the Interbedded-Type Shale-Oil Sweet Spots of Qingshankou Formation in Changling Depression

Liang Yang [1], Jilin Xing [1], Wei Xue [1], Lehua Zheng [2], Rui Wang [2] and Dianshi Xiao [2,*]

[1] Exploration and Development Research Institute, PetroChina Jilin Oilfield Company, Songyuan 138000, China; yang-liang@petrochina.com.cn (L.Y.); xing-jl@petrochina.com.cn (J.X.); lukn@petrochina.com.cn (W.X.)
[2] School of Earth Sciences, China University of Petroleum (East China), Qingdao 266580, China; s22010121@s.upc.edu.cn (L.Z.); s22010125@s.upc.edu.cn (R.W.)
* Correspondence: xiaods@upc.edu.cn

Abstract: Different types of shale-oil sweet spots have developed and are vertically stacked in multiple layers of the Qingshankou Formation in the Changling Depression, southern Songliao Basin. Furthermore, this area lacks a classification standard in the optimization of its shale-oil sweet-spot area/layers. Through relevant tests of the region in question's organic geochemistry, physical properties, oiliness, and pore structure, this paper investigates the formation elements of shale-oil sweet spots. In addition, summaries of its enrichment-controlling factors are given, and the classification standard and evaluation method for understanding the comprehensive sweet spots of the interbedded-type shale oil are then established. The interbedded-type shale oil is enriched in the Qingshankou I Member in the Changling Depression, and it has the features of medium-to-high maturity, the development of inorganic pores and micro-cracks, as well as higher oil saturation and better oil mobility. The sweet-spot enrichment is affected by lamina type, sedimentary facies, maturity, and sand–shale combinations. Both silty-laminated felsic shale and argillaceous-laminated felsic shale, which are developed in semi-deep lakes, are favorable shale lithofacies as they have excellent brittleness and oil mobility. The high maturity and the interbedded combination of sand and shale ensure the efficient production of shale oil, among which the pure-shale section issues a continuous contribution to the production process. Combined with oil testing, sweet-spot classification standards and a comprehensive evaluation of interbedded-type shale oil were established. An area of 639.2 km^2 for the interbedded-type shale-oil sweet spots was preferred, among which type I (193 km^2) belonged to the combination of "good shale and good siltstone interlayers adjacent", and type II belonged to "good shale and medium siltstone interlayers adjacent" combination (which have long-term low and stable production prospects). The research provides theoretical guidance on the effective exploration and development of the shale oil of the Qingshankou Formation in the Changling Depression.

Keywords: sweet-spot features; enrichment-controlling factors; interbedded-type shale oil; Qingshankou Formation; Changling Depression

Citation: Yang, L.; Xing, J.; Xue, W.; Zheng, L.; Wang, R.; Xiao, D. Characteristics and Key Controlling Factors of the Interbedded-Type Shale-Oil Sweet Spots of Qingshankou Formation in Changling Depression. *Energies* **2023**, *16*, 6213. https://doi.org/10.3390/en16176213

Academic Editor: Hossein Hamidi

Received: 3 July 2023
Revised: 18 August 2023
Accepted: 22 August 2023
Published: 26 August 2023

1. Introduction

Shale oil is one of the most important unconventional hydrocarbon resources that accumulates in organic-rich mud shale, as well as in its adjacent siltstone and carbonate rock interlayers in adsorbed and free states (where the single interlayer thickness should be less than 3 m, and the sum of the interlayers accounts for less than 20% [1,2]). Shale oil in China is mostly formed in continental deposition, and it is generally characterized by lower maturity, higher clay content, higher oil viscosity, and lower gas–oil ratios [2,3], thereby showing worse resource quality. However, with the improvement of horizontal well drilling, fracturing technology, and CO_2-enhanced oil/gas recovery technologies [4] (including CO_2

displacement and CO_2 prefracturing), successful breakthroughs have been made in recent years in the exploration of the three types of shale oil, which includes the interbedded type, mixed type, and pure-shale type [2,5]. Furthermore, the enrichment model and sweet-spot classification standard applicable to the continental shale oil in China have also been gradually formed [5,6]. The interbedded type of shale oil is represented by the Triassic Chang 7 Formation of the Ordos Basin, of which the sweet spots are mainly enriched in the siltstone interlayer adjacent to the organic-rich shale [7], whereby the mud shale contributes secondarily to the production capacity. The mixed type is represented by the Permian Lucaogou Formation in the Jimsar Depression, of which the dolomitic siltstone, sandy dolomite, and other mixed deposition rocks are the main sweet spots [8]. Its advantage is in its source reservoirs being interbedded, and source rocks such as dolomitic mudstone and shale contribute particularly little to production capacity. The pure-shale type is represented by the Upper Cretaceous Qingshankou Formation of the Gulong Depression in the northern Songliao Basin [9], where shale oil is mainly accumulated in the organic-rich shale matrix and bedding fracture. Moreover, its higher maturity (R_o > 1.2%) is a benefit in being the best match in terms of porosity, oil content, pressure, gas–oil ratio, and brittleness [9–11].

The Qingshankou shale oil of the Changling Depression, located in the southern Songliao Basin, contains the interbedded type and pure-shale type [12]. The interbedded type is mainly distributed in the Daqingzi area in the southern Changling Depression, and it is going through an experimental stage in the horizontal well development of shale oil, with the highest multilayers combined to a testing level of 20 t/d. Long-term exploration practice shows that the interbedded type of shale oil in the Changling Depression is different from other shale-oil exploration areas in terms of enrichment pattern and development mode; this is because it is deposited in the outer delta front environment [13]. The effective thickness of the siltstone interlayer is thin, which means it is difficult to achieve economic development with it alone. Meanwhile, the pure-shale section shows good potential (up to 14.6 t/d in the oil testing), thus revealing that the pure-shale section should provide an important contribution to the development of interbedded-type shale oil. The "sand and shale co-development" model effectively increases the horizontal well production capacity. Therefore, the joint contribution of the siltstone interlayers and adjacent shale should be considered in establishing the sweet-spot classification standard and in determining the best target layers of the horizontal well. However, this type of work has not yet been systematically carried out, which restricts the effective development of interbedded-type shale oil in this area. In addition, compared with the Qingshankou shale oil of the Gulong Depression [10], the shale oil of the Changling Depression has more diverse lithofacies [11] and a medium maturity [12]. The shale oil of these two areas are evidently different in terms of their reservoir characteristics, oil-bearing properties, and mobility [12,13]; therefore, the Gulong shale-oil sweet-spot standard is not appropriate as a guide for the sweet-spot preference of the interbedded-type shale oil in the Changling Depression.

As such, by using the lithology, geochemistry, physical properties, oil content, and other test results, this paper systematically evaluates the characteristics of sweet-spot enrichment elements, such as the petrography, physical properties, oiliness, and brittleness, of the interbedded-type shale oil of the Qingshankou Formation in the Changling Depression. Moreover, in this study, the key controlling factors of the formation of interbedded-type shale-oil sweet spots are summarized, and the sweet-spot optimization standards are then established by considering the joint contribution of the siltstone interlayer and pure-shale sections so as to provide a basis for the development of the interbedded-type shale oil in this area.

2. Basic Geological Features and Experimental Methods

2.1. Basic Geologic Features

The Songliao Basin includes four primary tectonic units, i.e., the Central Depressional Zone, the Western Slope Zone, the Eastern Uplift Zone, and the Southwest Uplift Zone (Figure 1a) [13], which are subdivided into 12 secondary tectonic units. The Changling De-

pression, located in the south of the Central Depressional Zone and connected to the Gulong Depression to the north, is a northeast-trending broad and gentle depression (Figure 1b) with an area of approximately 6500 km^2. Furthermore, it is the main area of conventional and unconventional oil and gas explorations in the southern Songliao Basin [13].

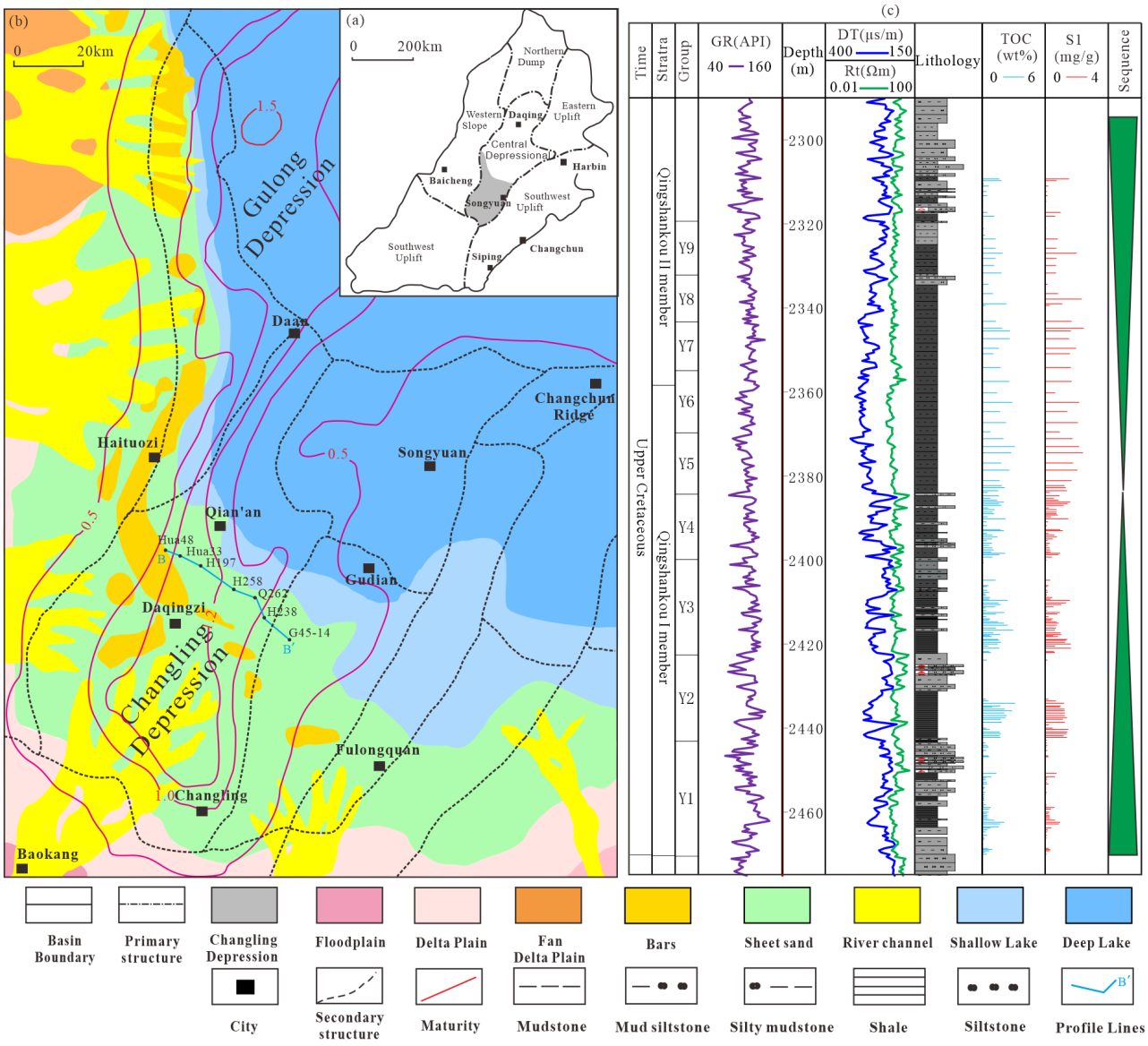

Figure 1. Tectonic location and the stratigraphic column (H258) of the Qingshankou Formation in the southern Songliao Basin. (**a**) Tectonic location of Songliao Basin; (**b**) Sedimentary facies distribution of Qingshankou I Member in the southern Songliao Basin; (**c**) the stratigraphic column of Qingshankou I Member (Well H258) in the Changling Depression, southern Songliao Basin.

The Upper Cretaceous Qingshankou Formation of the Changling Depression is divided into the Qingshankou I, II, and III Members. These are deposited in a pattern of "a central deep lake surrounded by delta", whereby the water bodies decrease from the Qingshankou I Member to the II and III Members (Figure 1b). The Qingshankou Formation is dominated by gray and gray-green mudstone with interlayers of siltstone and argillaceous siltstone (Figure 1c), which have a stratigraphic thickness of 250–550 m [12]. A large-scale water flooding occurred in the Qingshankou I Member, and the water bodies are widely spread and deeper. There are thick layers of organic-rich dark mud shale, which are deposited with a thickness of 80–100 m. During the deposition period of the Qingshankou Formation,

the southwest Tongyu-Baokang provenance was developed with a direction that is parallel to the long axis of the basin. In addition, its deposition range could be as far extended as to the areas of the Daqingzi and Qian'an regions, which form thin sand bodies that are deposited in the outer delta front and are adjacent to the dark mudstone that is deposited in a semi-deep lake. These features lead to a combination of "sand-in-shale" and to the development of interbedded-type shale oil.

The source-rock quality of the Qingshankou I Member shale in the Changling Depression is better than that of the II and III Members. The organic matter of the Qingshankou I Member mainly originates from laminar algae, mostly of type I and II_1 [14]. It has a high organic matter content (a TOC within the main range of 2–6%) (Figure 1c). The Qingshankou shale in the Changling Depression has a relatively high maturity (a R_o within the main range of 0.9–1.36%) (Figure 1b), albeit one that is slightly lower than that of the Gulong Depression [14,15]; however, it still shows a better shale-oil development prospect. At present, shale-oil sweet spots in this area are mainly concentrated in the lower Qingshankou I Member area (Group Y1, Y2, and Y3) (Figure 1c). Moreover, it has a favorable area of 2520 km^2, and two types of shale oil have developed, including the interbedded type and the pure-shale type. Among these, the interbedded-type shale oil is mainly distributed in the southern Changling Depression (i.e., Daqingzi region), and it changes to a pure-shale type toward the north. The interbedded-type shale oil of the Changling Depression has undergone a long-term exploration process. Before 2018, the exploration stage was mainly ongoing in the lithological reservoir. There, small-scale fracturing of the sandstone interlayers was being carried out, and it was producing poor single-well benefits. After this, the exploration concept was guided by the interbedded-type shale oil, and 28 vertical wells (which included 16 of the interbedded type and 12 of the pure-shale type) were performed, which achieved a higher shale-oil production with a daily oil testing of 0.3–20 t. After 2021, the interbedded-type shale-oil horizontal wells entered the developmental experiment stage, in which two horizontal wells were experimented on with a daily oil testing of more than 14 t. These experiments revealed that the Qingshankou shale oil in the Changling Depression has a broad shale-oil development prospect.

2.2. Samples and Experimental Methods

A total of 27 shale samples and 10 siltstone interlayer samples from the Qingshankou I Member in the Changling Depression were selected. Among these, the shale samples were collected from Wells H82GP1-24, H197, H81-39-15, and G45-14 (Table 1), and the siltstone interbedded samples were obtained from Wells Q1, Q5, Q6, H59, H60, H62, H72, and H104 (Table 2). The shale samples were tested using TOC, pyrolysis, XRD, thin-section observation, SEM, porosity and permeability, fluorescence scanning, laser confocal microscopy, and 2D NMR methods. These were performed to study the geochemical characteristics, rock composition, lithologies, pore structure, physical properties, oiliness, and mobility of the shale, respectively. The siltstone interbedded-type samples were tested for porosity, permeability, and mercury intrusion to study their physical properties and pore-throat structure. Furthermore, a distillation was conducted to study its oiliness. The above experiments were conducted in the Deep Oil and Gas Key Laboratory of China University of Petroleum (East China). The main test methods and steps are as follows:

2.2.1. TOC, Pyrolysis, and XRD Tests

After pulverizing, acidifying, washing, and drying the samples, the total organic carbon (TOC) content of shale samples was calculated via a carbon and sulfur analyzer, and rock pyrolysis analysis was performed on Rock-Eval 7. For the pyrolysis tests, the shale samples were pulverized to a 100-mesh size, the temperature was ramped up at 25 °C/min, and the parameters—such as residual hydrocarbon (S1), pyrolysis hydrocarbon (S2), hydrogen index HI (S2 to TOC ratio), and the OSI index (S1/TOC)—were calculated. Mineral components were revealed by X-ray diffraction according to SY/T5163-2010 [16], in which the samples were crushed uniformly to a 200-mesh size and then filmed. The XRD

results were quantitatively calculated with the K-value method. The mineral type, grain size, and crystal structure affected the test results, and the XRD results were corrected with the chemical dissolution and gravity separation methods.

Table 1. Shale sample information selected in Qingshankou I Member in the Changling Depression.

Sample	Depth (m)	Well	TOC (wt%)	Quartz (%)	Feldspar (%)	Clay (%)	Siderite (%)	Dolomite (%)	Calcite (%)	Pyrite (%)
#1	2218.45	H82GP1-24	2.17	30.15	21.48	39.49	0.00	2.35	4.35	2.19
#2	2220.2	H82GP1-24	3.62	26.20	29.17	39.49	0.00	2.28	1.50	1.36
#3	2224.64	H82GP1-24	1.35	35.93	22.35	39.16	0.00	2.56	0.00	0.00
#4	2226.07	H82GP1-24	0.65	35.04	23.21	36.86	0.00	1.73	0.00	3.17
#5	2231.72	H82GP1-24	0.78	37.73	28.34	33.93	0.00	0.00	0.00	0.00
#6	2236.4	H82GP1-24	0.92	33.53	27.53	31.43	0.00	4.06	2.35	1.10
#7	2237.76	H82GP1-24	3.55	22.37	32.26	39.21	0.00	5.25	0.00	0.91
#8	2238.76	H82GP1-24	2.31	30.55	22.33	35.41	1.17	10.54	0.00	0.00
#9	2249.5	H82GP1-24	0.10	40.25	31.00	12.92	0.83	12.37	2.63	0.00
#10	2251.4	H82GP1-24	0.41	39.07	14.57	32.47	2.79	7.89	2.15	1.07
#11	2255.48	H82GP1-24	0.78	35.20	18.10	35.83	3.89	4.29	1.74	0.95
#12	2257	H82GP1-24	0.80	32.99	23.61	33.72	3.32	5.64	0.72	0.00
#13	2259.26	H82GP1-24	2.08	28.87	15.92	46.08	4.16	3.94	0.00	1.03
#14	2263.9	H82GP1-24	1.67	27.60	17.02	42.26	2.92	7.41	0.88	1.92
#15	2264.9	H82GP1-24	0.49	25.19	24.87	23.90	1.02	10.33	12.22	2.47
#16	2527.5	H197	2.34	28.77	24.53	43.55	1.24	1.91	0.00	0.00
#17	2555.7	H197	0.41	32.13	19.31	45.86	0.00	0.82	1.88	0.00
#18	2548	H81-39-15	1.98	24.05	25.29	48.38	0.00	1.19	0.00	1.09
#19	1670.5	G45-14	1.87	28.97	22.39	38.64	3.79	0.00	6.21	0.00
#20	1689.5	G45-14	4.74	24.20	22.58	38.98	0.00	7.23	3.98	3.04
#21	1694	G45-14	0.46	34.84	18.74	42.15	0.00	1.18	3.09	0.00
#22	1712.3	G45-14	1.58	28.53	17.15	45.26	0.00	0.00	3.33	2.03
#23	1691.04	G45-14	7.91	18.91	38.48	37.02	0.00	3.17	0.00	1.76
#24	1693.06	G45-14	2.64	23.62	16.40	50.17	0.00	1.24	6.39	2.18
#25	1697.74	G45-14	0.27	30.70	22.94	43.62	0.00	1.07	1.67	0.00
#26	1699.62	G45-14	0.42	30.47	24.55	39.99	0.00	1.73	3.26	0.00
#27	1714.8	G45-14	1.38	24.03	21.05	46.02	0.00	0.68	1.76	6.45

Table 2. Siltstone samples selected in Qingshankou I Member in the Changling Depression.

Sample	Well	Depth (m)	Permeability (10^{-3} μm^2)	Porosity (%)	Smax (%)	Pd (MPa)	We (%)
#S1	H72	2427.80	0.01	4.40	78.40	8.48	40.33
#S2	Q1	1636.27	0.23	8.00	11.67	34.51	34.81
#S3	Q6	1857.82	0.10	7.50	90.85	1.37	43.36
#S4	H59	2453.09	0.01	3.80	72.22	10.30	32.93
#S5	H60	2417.40	2.54	12.90	93.83	0.34	47.59
#S6	H60	2360.40	2.56	14.50	92.80	0.34	49.39
#S7	H62	2423.20	5.90	16.20	97.34	0.34	41.58
#S8	Q5	1511.00	0.28	9.10	90.32	0.70	36.30
#S9	Q5	2360.03	2.24	11.10	93.13	0.34	36.58
#S10	H104	2370.54	0.21	6.90	94.61	0.69	31.14

Notes: Smax—maximum saturation of mercury intrusion; Pd—displacement pressure of mercury intrusion, MPa; We—withdrawal efficiency.

2.2.2. Physical Properties and Pore-Structure-Related Experiments

A PoroPDP-200 instrument, made by the American Core Lab Company (Houston, TX, USA), was employed to measure, according to the Standard of GB/T 34533-2017 [17], the helium porosity and pulse permeability of the shale and siltstone samples. The porosity was measured by the helium expansion principle and calculated using Boyle's law, while the

permeability was measured by the pressure pulse decay method. For the siltstone samples, mercury intrusion was performed on a Micromeritics Auto Pore IV 9500 porosimetry, made by the Micromeritics (American), in accordance with GB/T 29171-2012 [18], in which the intrusion and extrusion curves were obtained, and the pore-throat size distribution was calculated by the Washburn equation [19]. The maximum intrusion pressure was set to 41.37 MPa and corresponded to a pore-throat radius of 17 nm.

Thin-section observations and a quantitative evaluation of minerals via scanning electron microscopy (QEMSCAN) were used to reveal the lithology, mineral fabric, lamina type, and sedimentary structure [20]. After washing the oil, as well as drying and argon ion polishing, an FE-SEM analysis was performed (according to SY/T 5162-2021 [21]) using a Zeiss Crossbeam 550 field emission scanning electron microscope, made by the Carl Zeiss Microscopy GmbH (Jena, Germany), to reveal the pore types and pore-size distribution.

2.2.3. Other Experiments

The original shale samples were processed into suitably shaped pieces of approximately 8–15 g, and they were tested by using 2D nuclear magnetic resonance (NMR) with IR-CPMG sequences according to SY/T 6490-2014 [22]. Based on a 2D NMR-related fluid indication chart [23,24], different types of fluid, including free oil, adsorbed oil, free water, and bound water, can be recognized. By combining the calibration between the NMR signal and the fluid mass, the volume of different types of fluids can be determined; in addition, the movable saturation (i.e., the free oil saturation) can then be calculated with the porosity. Laser scanning confocal microscopy can characterize the distribution of the light and heavy hydrocarbon components in shale samples, and it can effectively study the internal enrichment and transport mechanisms of hydrocarbons. Meanwhile, the fluorescent observation method was used to reveal the accumulation location of the residual oil in the shale samples. Oil saturation was measured by using a distillation method on the original shale and siltstone samples, in which the water contained in the core was evaporated, condensed, collected, and recorded. The core was removed from the oil, then dried and weighed. The oil and water saturation in the rock can be calculated with the porosity.

3. Characterization of the Shale-Oil Sweet-Spot Elements

3.1. Petrography

The TOC of the 27 shale samples ranged from 0.1% to 7.91%, with a mean value of 1.77% (Table 1). The major mineral that has developed is clay (meaning 38.6%), followed by quartz and feldspar, and calcite and dolomite have developed in small amounts (Table 1). The lithology of the Qingshankou I Member in the Changling Depression is more complex than that in the Gulong Depression [25]. According to the lithological classification standard of "organic matter abundant, sedimentary structure, and mineral composition" [26] and considering the laminae types related to the grain size (including the silty lamina that had a proportion of silty grain that was more than 50% in a single lamina, as well as the argillaceous lamina that was lower than 50%), the lithofacies of the Qingshankou I Member were mainly classified into six types (Figure 2). These included the organic-rich argillaceous-laminated clayey shale (type A), the medium-to-high organic argillaceous-laminated felsic shale (B), the medium-to-low organic silty-laminated felsic shale (C), the medium-to-low organic massive mudstone (D), the silty mudstone (E), and siltstone (F). The features of the main lithology are detailed as follows.

Both the type A and type B lithologies were rich in argillaceous laminae (Figure 2b,d), in which the silty laminae accounted for less than 10%. For type A, the core is commonly gray-black to black (Figure 2a), dark laminae develop with flat and continuous forms, and it has more clay minerals (>50%) and a higher TOC (>2%) than others. Furthermore, it is mostly deposited in deep lakes. For the type B shale, the core is dark-gray to gray-black (Figure 2c), the laminae develop with flat or discontinuous forms, and it has relatively low clay minerals (<50%) and a medium-to-high TOC ($\geq$1%). It is mostly deposited in semi-deep lakes or deep lakes. For type C, the core is dark-gray to gray (Figure 2e), silty laminae

account for 10–50% of its constitution, and it has rippled, continuous, or discontinuous forms (Figure 2f). Furthermore, it has a medium-to-low TOC (<2%) and is mostly deposited in semi-deep lakes or turbidity currents. For type D, the core is predominantly gray-dark to gray, it contains ostracoda and massive structures (Figure 2g), and it has a medium-to-low TOC (<2%). For type E, the core is gray-dark to gray, and it mainly develops massive structures (Figure 2j). Moreover, it is poor in TOC (<1%), and it is mostly deposited in the outer delta front or in shallow lakes. For type F, the core is gray with a development of partial argillaceous laminae (Figure 2l), and it is mostly deposited in the outer delta front.

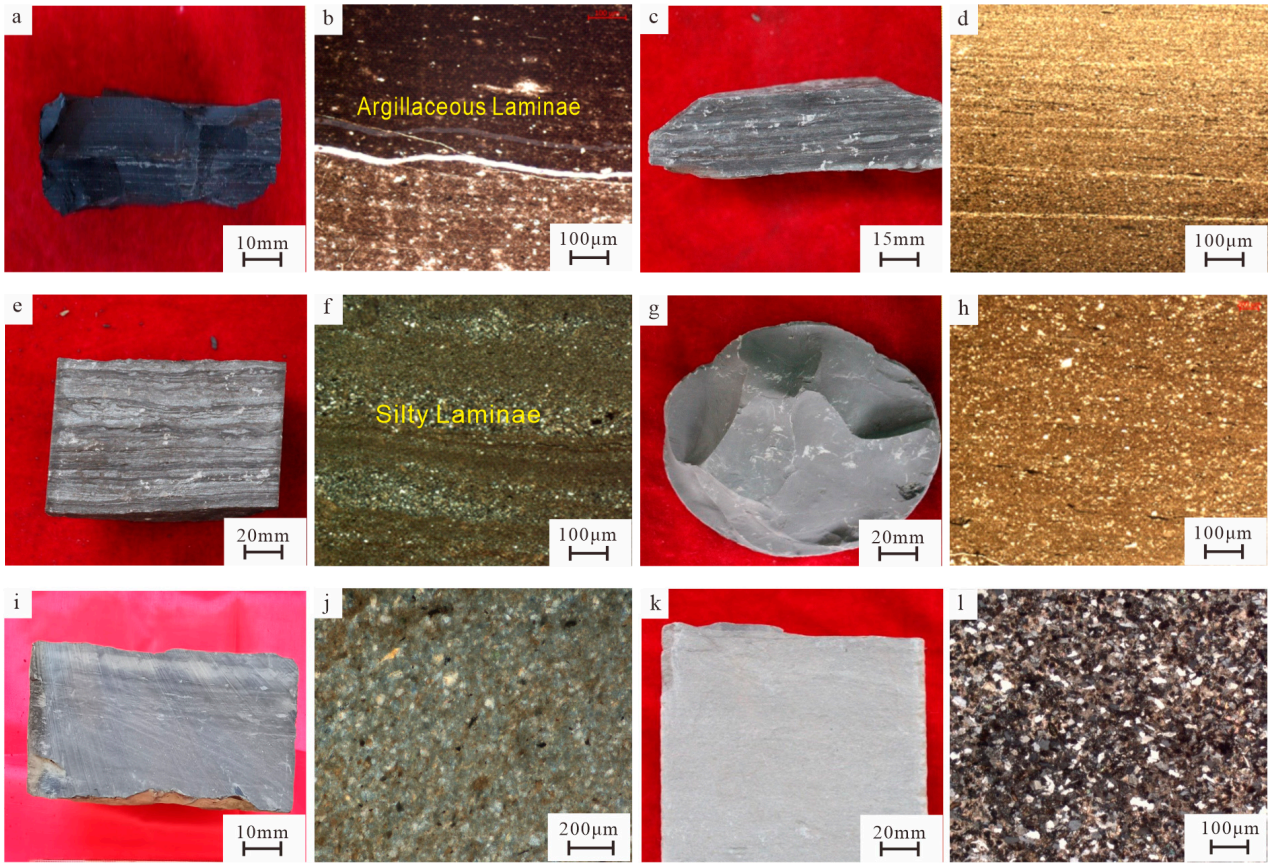

Figure 2. Core images and thin sections of the main lithofacies of the Qingshankou I Member in Changling Depression. (**a**) Core image of the argillaceous-laminated clayey shale, sample #13; (**b**) the thin section (single polarized light) of the argillaceous-laminated clayey shale, sample #22; (**c**) the core image, argillaceous-laminated felsic shale, sample #16; (**d**) the thin section (single polarized light) of the argillaceous-laminated felsic shale, sample #8; (**e**) the core image of the silty-laminated felsic shale, sample #5; (**f**) the thin section (single polarized light) of the silty-laminated felsic shale, sample #6; (**g**) the core image of the massive mudstone, sample #10; (**h**) the thin section (single polarized light) of the massive mudstone, sample #3; (**i**) the core image of the silty mudstone, sample #12; (**j**) the thin section (single polarized light) of the silty mudstone, H258, 2457.59 m; (**k**) the core image of the siltstone, sample #S3; (**l**) the thin section (single polarized light) of the siltstone, sample #S5.

3.2. Physical Properties of Shale-Oil Sweet Spots

The pores of the Qingshankou I Member shale samples are composed of five types, which include the intergranular pores, solution pores, intercrystalline pores, organic pores, and micro-cracks (Figure 3), among which the inorganic pores and micro-cracks play a major part.

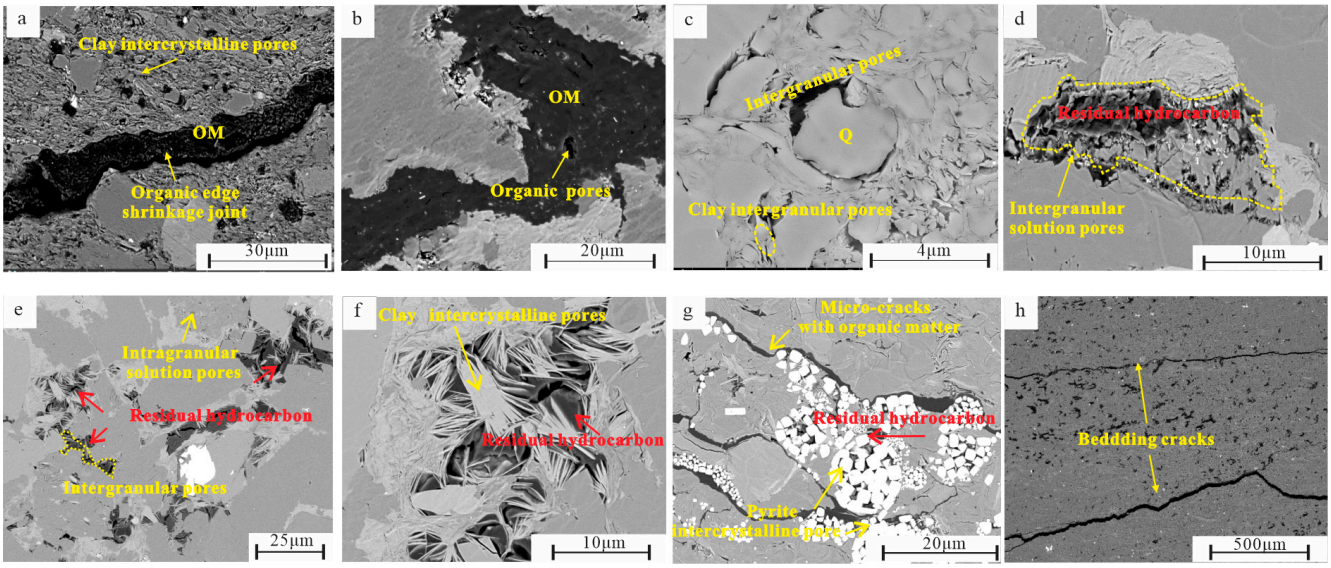

Figure 3. Pore microscopic features of shale-oil reservoirs of Qingshankou I Member in Changling Depression. (**a**) Clay intercrystalline pores and organic matter edge shrinkage joint, organic-rich argillaceous-laminated clayey shale #2; (**b**) organic pores, organic-rich argillaceous-laminated clayey shale #7; (**c**) intergranular pores between quartz and clay, argillaceous-laminated felsic shale #9; (**d**) felsic intergranular solution pores, enriched in residual hydrocarbon, argillaceous-laminated felsic shale, #18; (**e**) intergranular pores and intragranular solution pores, siltstone, #9; (**f**) clay intercrystalline pores with visible enrichment of residual hydrocarbons, silty-laminated shale, #14; (**g**) pyrite intercrystalline pores filled with residual hydrocarbons, micro-cracks filled with organic matter, argillaceous-laminated clayey shale, #22; (**h**) bedding cracks filled with organic matter, organic-rich argillaceous-laminated clayey shale, #19.

The development of organic pores is related to maturity [27]. As the R_o is lower than 1.2%, the organic pores are locally developed (but are less than 10% in terms of proportion), and they are mostly in the form of edge shrinkage joints or isolated large pores that are distributed in the center of the organic matter (Figure 3a,b). The intergranular pores are mostly residual pores between the quartz and feldspar particles (Figure 3c,e), and they are locally distributed between clay aggregates (Figure 3c) with regular edges and pore diameters that are larger than 500 nm (which is important for shale-oil accumulation in this area [28]). The solution pores are related to the dissolution of feldspar and carbonate minerals (Figure 3d), and both intra- and intergranular solution pores are visible with irregular morphologies. The intergranular solution pores are generally large, and the intragranular solution pores are mostly less than 500 nm (Figure 3e) and isolated. The intercrystalline pores are widely developed in between the crystals of the clay minerals (Figure 3a,f), pyrite (Figure 3g), quartz microcrystals, etc., with pore diameters that are concentrated in the 50–200 nm range. The intercrystalline pores are commonly filled by residual hydrocarbon, especially for pyrite intercrystalline pores (Figure 3g). The micro-cracks are particularly well developed in the shale, and they are dominated by bedding cracks that range from a few to tens of μm in width. Moreover, they are often filled with quartz microcrystals or organic matter (Figure 3h), thus providing a dominant channel for shale-oil seepage [11].

The helium porosity of the shale samples varied in the range of 3.4–8.4%, and the horizontal permeability reached as high as 0.1–1 mD, which is 100–1000 times the vertical permeability and is due to the development of bedding cracks. Moreover, it has a weak correlation between porosity and permeability. The pore-size distribution of the different types of laminae was quantitatively evaluated based on SEM images and energy spectroscopy (Figure 4) so as to guide the impacts of the laminae types on the development of pore space.

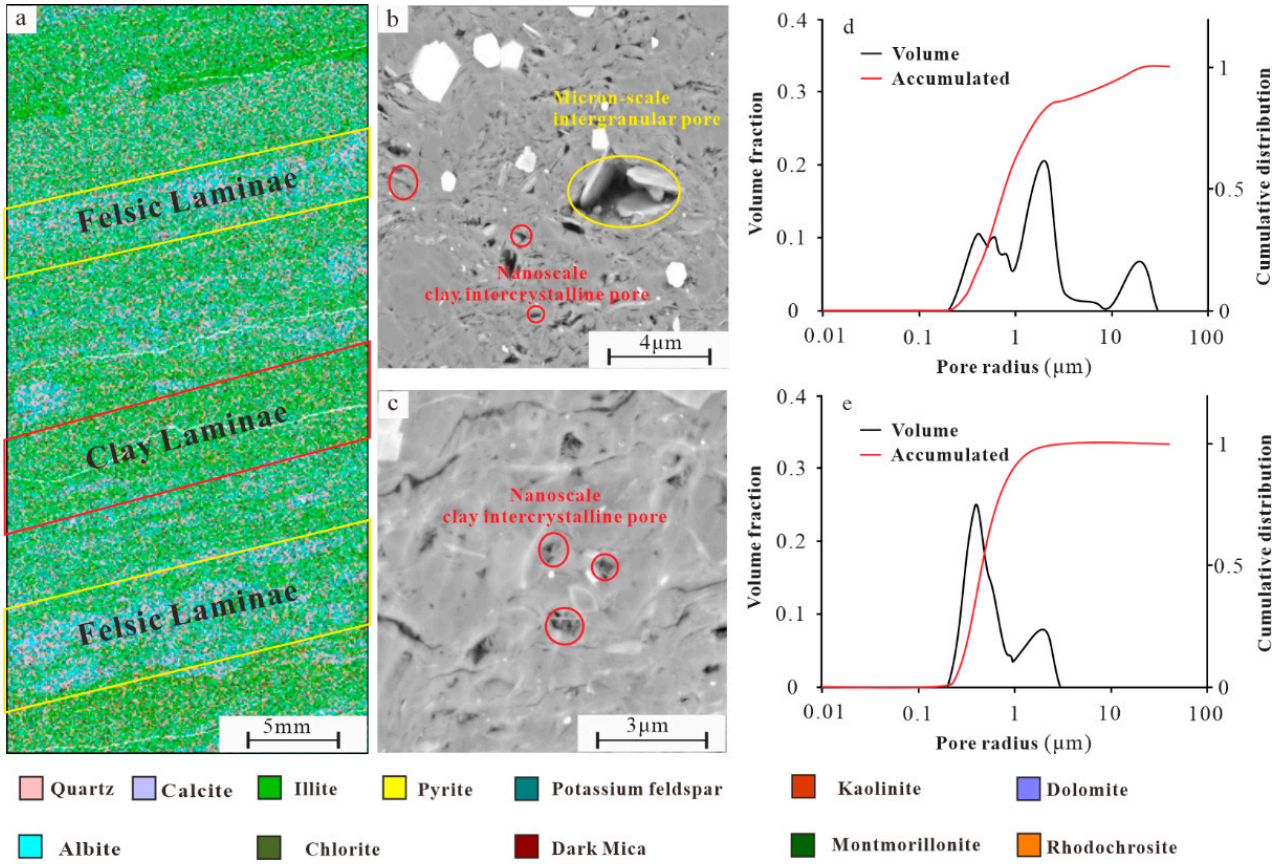

Figure 4. Pore development characteristics of different laminae types of Qingshankou I Member shale in Changling Depression. (**a**) QEMSCAN, interbedded felsic and clayey laminae, laminated felsic shale, #16; (**b**) SEM image of felsic laminae, micron-scale intergranular pores developed; (**c**) SEM image of argillaceous clayey laminae, nanoscale clay intercrystalline pores developed; (**d**,**e**) the pore-size distributions of felsic laminae and clay laminae based on the image method.

The argillaceous clayey laminae are dominated by intergranular pores and solution pores, followed by intercrystalline pores and organic pores. The pore-size distribution of these was broadened, with the main peak being in the range of 100–300 nm and the large pores (>1 μm) accounting for less than 20% (Figure 4c,e). Compared to the argillaceous clayey laminae, the intergranular pores were more developed in the silty laminae or felsic laminae. In these, the pore-size distribution became wider, with the main peak in the range of 1–3 μm and the large pores (>1 μm) accounting for around 40% (Figure 4b,d). Overall, the pore-size distribution of the Qingshankou I Member shale reservoir in this area is wide, and the large pores (>1 μm) are more developed than that of the Gulong shale reservoir [15], which thus provides a high-quality reservoir for shale oil [29]. Therefore, silty-laminated shale and argillaceous-laminated felsic shale are the favorable shale lithologies of the Qingshankou I Member.

Compared with pure shale, the physical properties of the siltstone interlayer of the Qingshankou Formation were significantly better, with a porosity ranging from 3.5% to 16.2% (the average value being 9.4%) and a permeability ranging from 0.01 to 5.9 mD (the average value being 1.4 mD). The siltstone interlayer could be classified into four types according to the mercury intrusion curves (Figure 5), namely types I, II, III, and IV.

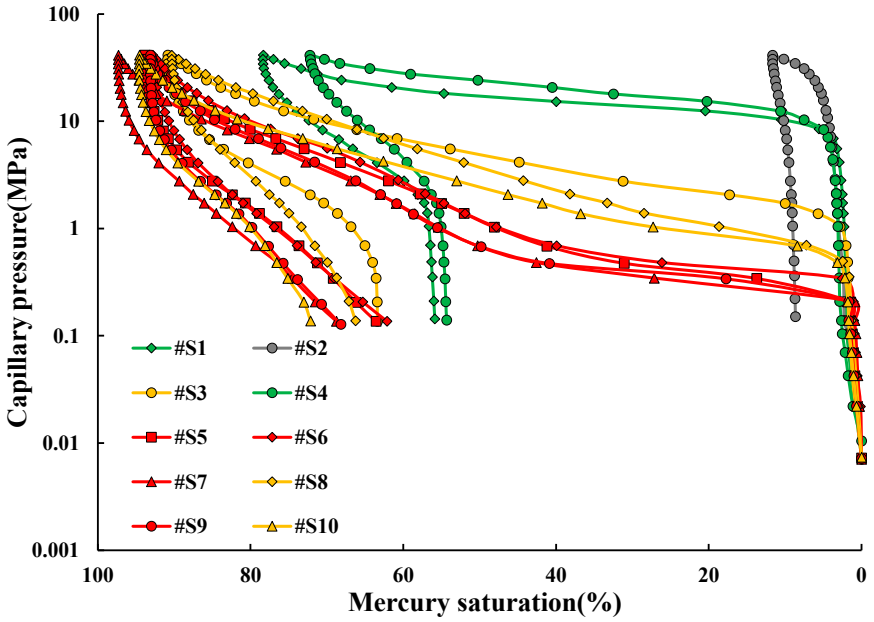

Figure 5. Characteristics of the mercury intrusion curves of four types of siltstone interlayer reservoirs of the Qingshankou I Member in Changling Depression.

The type I reservoirs (red line in Figure 5) had a concave-shaped intrusion curve, lower displacement pressure (<0.35 MPa), and a higher mercury withdrawal efficiency (averaging 37%), which corresponded to a higher porosity (greater than 11%) and an intergranular pore-throat system that dominated in this type of reservoir [30]. The type II reservoirs (yellow line in Figure 5) had a medium displacement pressure (<1.37 MPa), medium porosity (>9%), and a developed solution pore-throat system [31]. The mean value of the displacement pressure of the type III reservoir (blue line in Figure 5) was mostly higher than 10 MPa, and the solution and the intercrystalline pore-throat system were dominant. Therefore, the type I and II reservoirs had the best pore-throat structure, and they were the most favorable siltstone interlayer reservoirs.

3.3. Oil-Bearing Characteristics of the Shale-Oil Sweet Spots

According to the pyrolysis experiments of the shale samples, the free hydrocarbon S1 of the Qingshankou I Member ranged from 0.5 to 6 mg/g, of which the samples greater than 2 mg/g accounted for 61% and showed good oiliness (Figure 6).

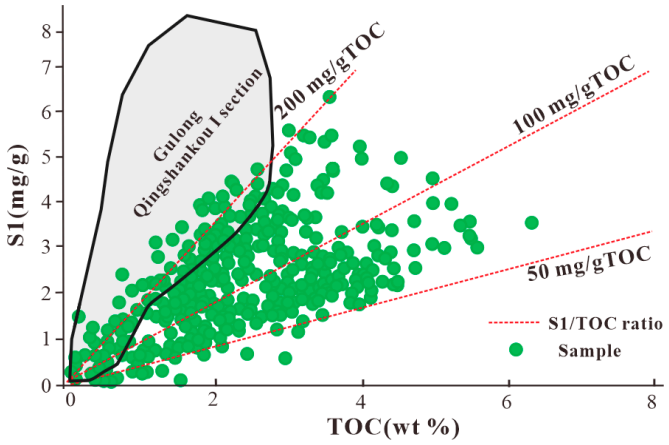

Figure 6. Relationship between organic matter content and S1 of Qingshankou I Member in Changling Depression.

The S1 value and TOC were positively correlated, and the S1/TOC ratio was generally higher than 50 mg/g TOC. Of these, samples that had more than 100 mg/g TOC accounted for over 50%, which is slightly lower than that of the Gulong shale oil [11] (Figure 6). Based on the distillation method, the oil saturation of the shale samples ranged from 43% to 78%, with an average value of 57%, which is comparable to the Gulong shale oil [15]. Overall, the oil saturation was positively correlated with the TOC and clay, and the organic-rich argillaceous-laminated clayey or felsic shale contained the largest amount of oil. The saturated and aromatic hydrocarbons in the crude oil accounted for 79%, thus revealing the higher movable hydrocarbons in the shale oil of the Qingshankou I Member in the Changling Depression.

The percentage of the swelling state of the shale oil gradually decreased with increasing maturity [32], and when the $R_o > 1\%$, then the shale oil was mainly in the adsorbed and free states [29]. Based on the quantitative evaluation of the shale oil in different states of sealed in situ samples via 2D NMR [29], the saturation of free oil ($T_2 > 1$ ms, $100 > T_1/T_2 > 10$) varied from 5.3% to 75.1%, with a mean value of 36%, which is significantly higher than that of the adsorbed oil (averaging 21%). Furthermore, the percentage of free oil was significantly higher contained in the silty-laminated shale than in the argillaceous-laminated shale. There were differences in the accumulation characteristics of the shale oil in the different types of laminae (Figure 7).

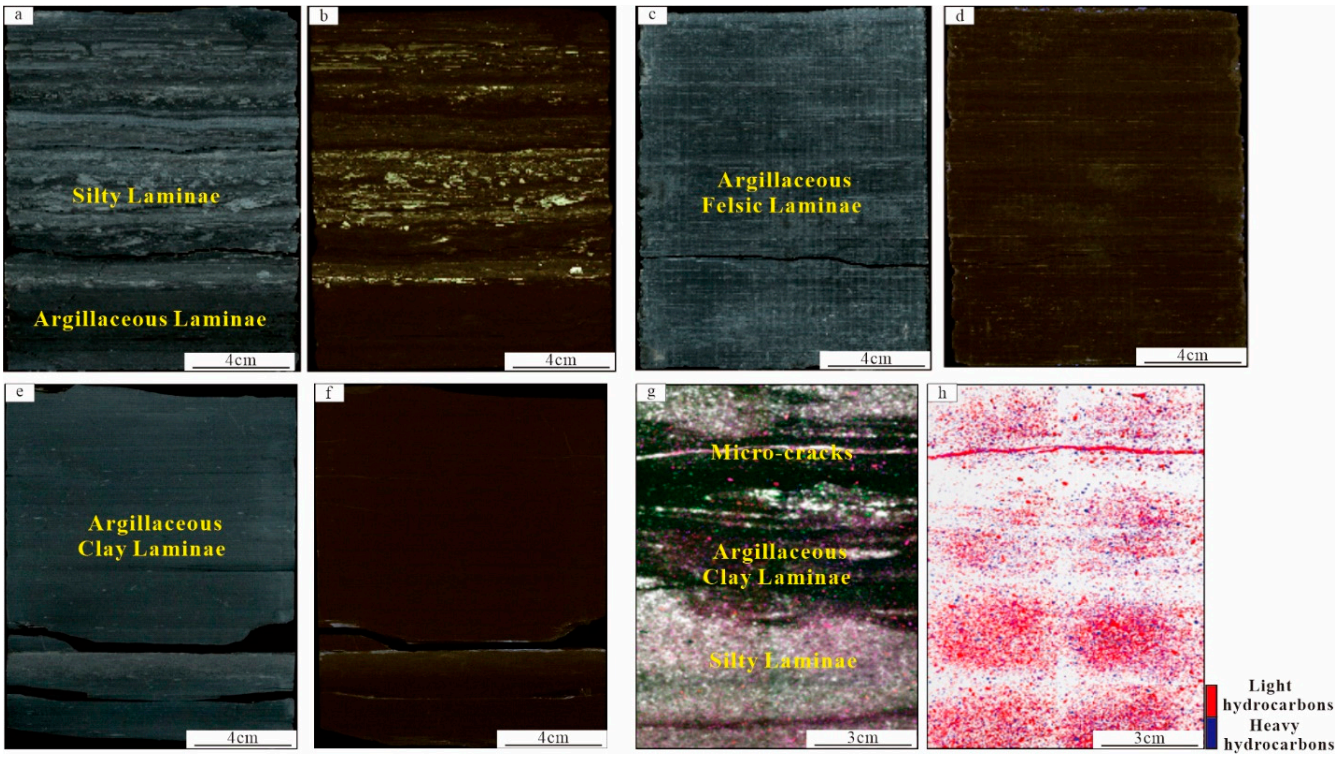

Figure 7. Oil-bearing fluorescence display of different shale lithofacies of Qingshankou I Member in Changling Depression. (**a**) Core image (white light) of the medium organic silty-laminated felsic shale, #27; (**b**) the fluorescence image of (**a**), where a yellow fluorescence exists in the silty laminae; (**c**) the core image (white light) of medium-to-high organic argillaceous-laminated felsic shale, #21. (**d**) The fluorescence image of c with poor fluorescence; (**e**) the core image (white light) of the organic-rich argillaceous-laminated clayey shale, #13; (**f**) the fluorescence image of e, where poor fluorescence was displayed within the clayey laminae; (**g**) the fluorescence image of the silty-laminated felsic shale, #24; (**h**) the laser confocal scanning of (**g**), whereby light (red) and heavy hydrocarbon components (blue) had developed.

The silty laminae and bedding cracks were generally oil-rich with yellow or orange fluorescence (Figure 7b), indicating that more light components are inclined to exist in the free states of the intergranular pores, intergranular dissolution pores, or micro-cracks (Figures 3 and 7h). Meanwhile, the argillaceous-laminated shales contained the highest oil content but also had the weakest fluorescence display (Figure 7e,f), thus indicating that a higher percentage of a heavy fraction of oil accumulates in argillaceous laminae and is mostly in the adsorbed state on the surface of clay minerals and organic matter (Figures 3a and 7h).

On the one hand, the difference in oiliness between the adjacent laminae was related to the difference in mineral composition and the pore space of the different types of laminae. On the other hand, it can be attributed to the micromigration of the shale oil between laminae as many of the light hydrocarbon components were migrated, through bedding cracks [33], from the organic-rich argillaceous laminae migrates to the adjacent silty laminae shale or felsic laminae.

4. Main Controlling Factors of the Shale-Oil Sweet-Spot Enrichment of the Qingshankou I Member in the Changling Depression

4.1. Favorable Shale Lithofacies

From the south to the north of the Changling Depression, the deposition environment of the Qingshankou I Member gradually changes from the outer delta front to the deep lake. This leads to a transformation of the "type F-C-B" lithology combination to the "type B + A + C" and "type A + B" combinations in the north (Figure 8), thus showing the decrease in type F and type C, as well as an increase in type B and type A. From the bottom to the top, the water in the Qingshankou I Member deposition period gradually increased in stability, the proportion of type F and type C gradually decreased, and type B and A increased (Figure 8). In the southern Changling Depression, the water in the lower Qingshankou I Member (namely the Y1–Y3 groups) frequently fluctuated, leading to the development of a type F that is adjacent to type C or type B (Figure 8), which is of benefit in the development of the interbedded-type shale oil.

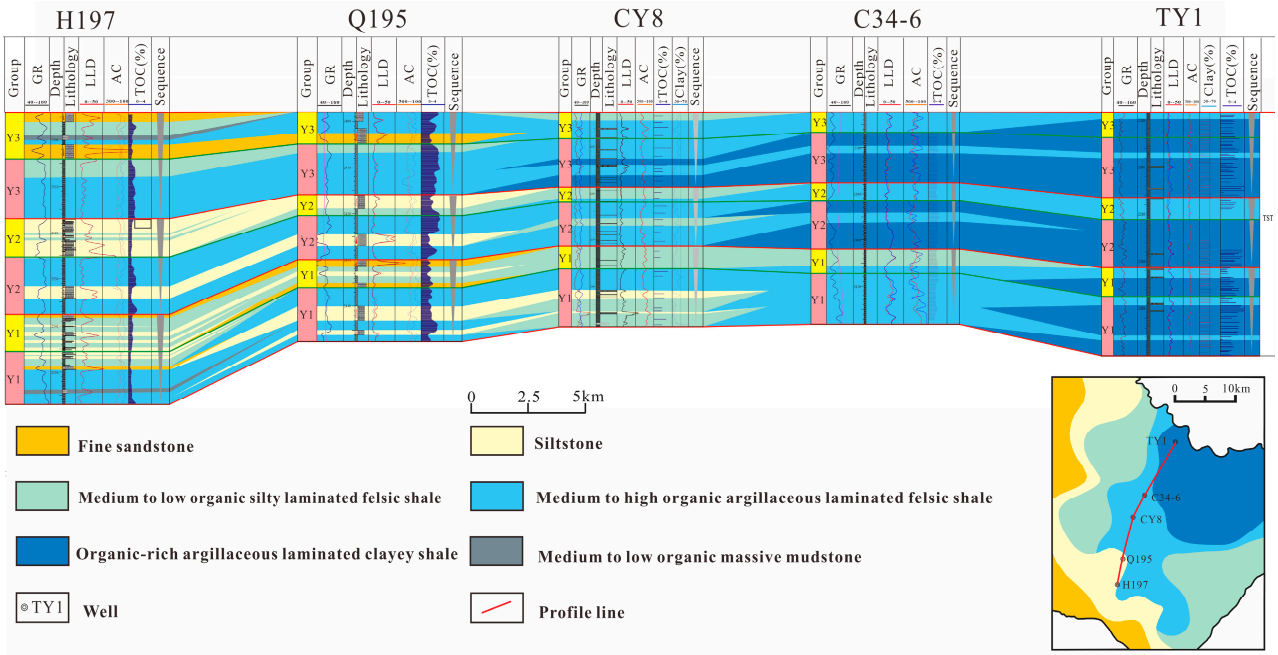

Figure 8. The lithology distribution profile of Qingshankou I Member in Changling Depression.

According to the analysis of the physical properties and oil-bearing properties of different types of shale, it can be concluded that silty-laminated felsic shale and argillaceous-laminated felsic shale are the favorable shale lithofacies. These lithofacies are closely

related to higher content of felsic minerals, a close interbedding with organic-rich laminae, and the development of high-density laminae. Firstly, the mean content of the felsic minerals in these two types of lithofacies can be up to 62%, and a quartz with a coarse-grain size is developed, which mainly comes from a terrestrial source. This leads to forming a brittle framework in the shale matrix, which can then benefit in protecting the pores from compaction [34]. With the increase in felsic minerals, the effective porosity became better (average 5.8%) (Figure 9a), and these two shale lithofacies had more residual intergranular pores with a micron size, which in turn provides a high-quality reservoir space for shale oil [13].

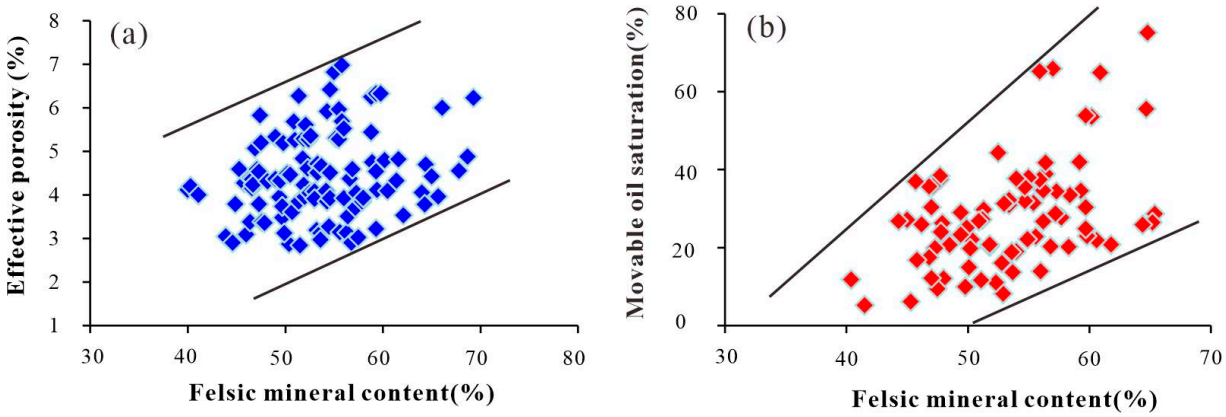

Figure 9. Correlation of the felsic mineral content with effective porosity (**a**) and movable oil saturation (**b**) of Qingshankou I Member in Changling Depression.

The core images and thin-section observations showed that silty laminae and felsic laminae are commonly interbedded with organic-rich clayey laminae, and the thickness ratio of felsic laminae to clayey laminae is about 1.63 (Figure 4a). Clayey laminae have a higher TOC [14,35] and stronger hydrocarbon generation, but nanoscale pores dominated due to the plastic–mineral matrix. Through the molecular dynamics simulation method [36], many researchers have studied the microscopic interaction mechanism between hydrocarbons and minerals and have realized that crude oil components and mineral types have an evident control over adsorbed oil. Organic matter has the strongest adsorption capacity for hydrocarbons, followed by clay minerals, and the heavier the crude oil components are, the easier it is to be adsorbed [37]. Therefore, the heavy hydrocarbon component is preferentially adsorbed on the surface of clay minerals and organic matter [38], while the light hydrocarbon component has better mobility and is prone to migrate vertically to adjacent silty laminae or felsic laminae through the micron channels (such as cracks) [39,40], thus resulting in the enrichment of light hydrocarbon components in silty-laminated shale and felsic shales. Therefore, with an increase in the felsic mineral content, the movable oil saturation increases (Figure 9b). In addition, the mean laminae density of these two lithofacies can reach 197/m. When this occurs, many bedding cracks develop [13], which can effectively improve the seepage of the shale oil through its interaction with hydraulic fracturing [41].

A higher content of felsic minerals is also beneficial for later fracturing [1,2]. The laboratory rock mechanics experiment shows that silty-laminated shale has a higher Young's modulus (22.82 Gpa) and a lesser Poisson's ratio (0.12), and this is followed by felsic shale. Clayey shale has the lowest Young's modulus (4.84 GPa) and the highest Poisson's ratio (average 0.2), corresponding to the worst fracturability [42]. Therefore, it is clear that both silty-laminated shale and argillaceous-laminated felsic shale have better physical properties, mobility, and fracturability, and they are the most favorable shale lithofacies of the Qingshankou I Member in the Changling Depression.

4.2. The Control of the Sedimentary Environment on the Favorable Shale Lithofacies

During the sedimentary period of the Qingshankou Formation, a turbidity current developed over a wide area [43]. The gravity slip caused the sand body deposited in the delta front to transport again, and as the bed loaded, it grew and was transported along with the argillaceous clay flocculation at the lake bottom for a long distance [44]. With the decrease in flow velocity, the silty laminae were first deposited, and the argillaceous flocculent ripples continued to move downstream; furthermore, it was deposited with less velocity. After deposition and compaction, sedimentary structures such as sandballs and water escape can be seen. At the same time, the turbidity current brought a large amount of oxygen and had a certain consumption effect on the organic matter. The turbidity current dominated the formation of the medium-to-low organic silty-laminated felsic shale; thus, it was developed in the center of the Changling Depression, near the semi-deep lake area (Figure 10).

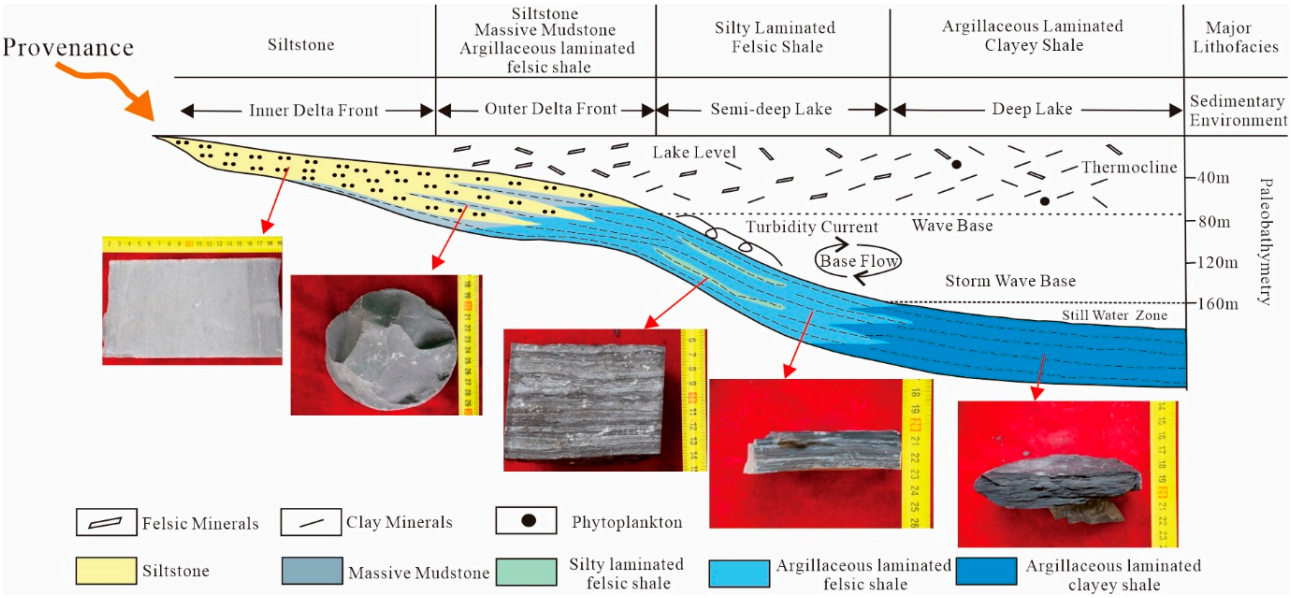

Figure 10. Shale lithofacies development models of Qingshankou I Member in Changling Depression.

In the semi-deep lakes to the deep lakes, the deposition environment of the water was evidently stratified [44]. Many of the argillaceous felsic grain, clays, and phytoplankton were suspended in the thermocline, among which the felsic minerals migrated, via circulation and mixed diffusion, from the provenance. The changes in climate, temperature, and salinity would make the thermocline disappear [34,44] and destroy the equilibrium state of the stratification. The suspended matter then begins to settle with different deposition rates (felsic mineral > clay) [45], thus leading to the formation of argillaceous laminae, which are related to the season and climate. The closer to the provenance, the more sufficient the supply of felsic minerals and the higher the oxygen content is (which has a certain consumption effect on organic matter [46]). This led to the formation of the medium-to-high organic argillaceous-laminated felsic shale to be widely distributed in the semi-deep lake area (Figure 10). In the deep lake environment, the further away from the provenance, the less there was a supply of felsic minerals, and it is here that the organic-rich argillaceous-laminated clayey shale developed.

4.3. The Key Control of High Maturity on the Enrichment and High Yield of Shale Oil

With the increase in maturity, the heavy components generated by hydrocarbon generation from organic matter gradually begin pyrolysis. In addition, the light components increase, leading to a decrease in the density and viscosity of crude oil, as well as an increase in the gas–oil ratio [6,29]; moreover, the mobility of shale oil also becomes better. Figure 11

shows the variation of geochemical parameters, crude oil density, and gas-to-oil ratio with maturity of the shale of the Qingshankou I Member in the Changling Depression. When the R_o is up to 0.7%, the S1 + S2 and HI index (S2/TOC) begin to decrease rapidly, indicating that the hydrocarbon expulsion threshold is being entered. During this period, the crude oil density is >0.85 g/cm^3. When the R_o > 1.0%, the OSI index (S1/TOC) begins to increase and can reach 300 mg/g TOC. During this period, the mobility of shale oil gets better, the oil density decreases to 0.85 g/cm^3, and the gas–oil ratio can reach 20 m^3/m^3. When maturity is higher than 1.2%, the density of shale oil is less than 0.85 g/cm^3, and the gas–oil ratio is higher than 50 m^3/m^3. When this occurs, the light hydrocarbon component is developed, and the mobility is at its best [47].

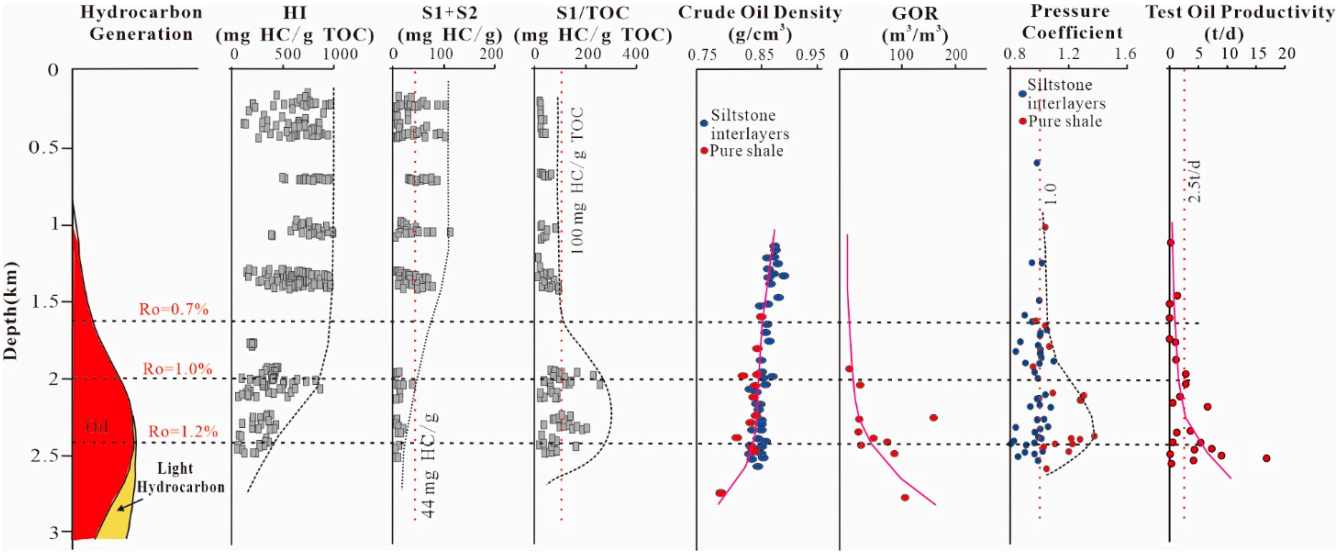

Figure 11. Variation of geochemical parameters, crude oil density, gas-to-oil ratio, pressure coefficient, and test oil productivity with the maturity of Qingshankou I Member in Changling Depression. HI-S2/TOC; GOR—gas-to-oil ratio.

In addition, the pore-pressure coefficient of shale is also controlled by maturity, and with the increase in thermal evolution, the hydrocarbon generation pressurization effect becomes obvious [15]. When the R_o is greater than 1.0%, a high over-pressure is commonly developed in shale, and the pressure coefficient is in the range of 1.2–1.38 (Figure 11). Over-pressure provides sufficient power for shale-oil flow. It can be seen that maturity affects the hydrocarbon generation evolution of shale, controls the shale-oil components and viscosity, and determines the mobility of the shale oil. When the maturity is greater than 1.0%, the oil testing increases significantly (>2.5 t/d) for both the pure-shale type and interbedded-type shale oil in the Changling Depression.

The oil saturation of the siltstone interlayers ranged from 3.2% to 75%, with a mean value of 38%, showing strong heterogeneity. The oil saturation of the siltstone interlayers is controlled by the reservoir quality, adjacent source quality, and the tectonic background. When the maturity is less than 0.9%, the siltstone interlayers have a lower oil saturation (<50%), which corresponds to poor oil testing; when it is greater than 0.9%, there is a significant increase in oil saturation (54–60%), indicating that the maturity has an important control on the oiliness of the siltstone interlayers. The higher the maturity of the source rock (i.e., shale), the stronger the hydrocarbon generation ability, and the greater the pressure difference between the source and reservoirs [38], which leads to a higher charging power and oil saturation in the adjacent siltstone interlayers. Under a similar source quality and tectonic background, the type I and II siltstone interlayers have a higher saturation than the other types.

4.4. A Good Combination of Sand–Shale Is Conducive to Efficient Development

The Qingshankou Formation in the Changling Depression is deposited in a lacustrine environment with frequent water fluctuations [43]. During the regression period, the distributary channels and sheet-sand microfacies in the outer delta front extended to the center of the lake, thus forming the siltstone interlayers or silty-laminated shale; during the water flooding period, organic-rich dark mud shale was deposited, forming the vertical siltstone and shale interbedding association. The siltstone interlayers have better physical properties, coarse grain, and higher brittleness, which is conducive to the vertical expansion of a hydraulic fracture network to the adjacent pure-shale-oil sweet spot, and provides a highway for shale-oil seepage. The microseismic monitoring of horizontal well Q265 after fracturing in the siltstone interlayers shows that the fracture expansion height is in the range of 21–39 m, with an average value of 32 m. Through fiber monitoring, fracturing fluid can extend 12.5 m upward along the perforated interval, and the fracture height is significantly higher than that of a pure-shale section (the hydraulic fracture height of Gulong shale is 6–9 m) [10].

There is generally normal pressure (pressure coefficient < 1.0) in the siltstone interlayers and over-pressure in the pure-shale section (Figure 11), and the pressure difference between these two sections is 4–7 MPa, which is conducive to the migration of the movable oil of pure-shale sections into the siltstone interlayers through fractures [48]. This ensures the long-term stable production of shale-oil wells. The horizontal well development practice of interbedded-type shale oil confirms the contribution of the pure-shale section. In the early stage of small-scale fracturing, the production of horizontal wells in siltstone interlayers is almost unaffected by the pure-shale section, and the oil intensity of stable production in the second year decreases to about 0.74 t/100 m. Through using large-scale fracturing in the later stage, the fracture is extended to the adjacent pure-shale section, and the stable production in the second year can reach 0.8–1.7 t/100 m, indicating that the contribution of the shale section to production can reach approximately 30%. Therefore, the co-development of siltstone interlayers and the pure-shale section is conducive to the efficient production of shale oil in the Changling Depression.

5. Interbedded-Type Shale-Oil Enrichment Laws and Its Exploration Direction of the Qingshankou I Member in the Changling Formation

The distribution of the interbedded-type shale-oil sweet spots of the Qingshankou I Member in the Changling Depression is controlled by the quality of the siltstone interlayers and shale section, and this is shown through the multilayer sweet spots being superimposed. Firstly, according to the oil testing of a single layer, the classification standard of the sweet spots of siltstone interlayers and the shale section were established (Table 3).

Among them, thickness, oil saturation, energy-storage parameters (the product of porosity, saturation, and thickness), and the structural background are preferred for the sweet spots of the siltstone interlayers, while the Ro, TOC, as well as the degree of brittle minerals, porosity, and lithofacies, are preferred for the pure-shale-oil sweet spot. According to the idea of "determining the zone distribution based on favorable area selected parameters and determining the intervals based on favorable layer selected parameters", the plane and vertical distributions of the sweet spots were carried out. The favorable area selected parameters were used to determine the sweet-spot distribution of the siltstone interlayer and pure-shale sections. Then, the three types of sweet spots of the interbedded-type shale oil were classified according to the superposition relationship of the sweet spots of the siltstone interlayer and pure-shale sections, among which the type I sweet spots corresponded to the combination of "type I siltstone interlayer and type I shale sweet spots", the type III sweet spots corresponded to the combination of "type III siltstone interlayer and type III shale sweet spots", and the remaining situations were of the type II sweet spots.

Based on shale-oil logging evaluation technology [49,50], the sweet-spot distribution of the shale oil of the Qingshankou I Member was characterized. Under the control of a

sedimentary environment, the shale-oil sweet spots of the Qingshankou I Member in the Changling Depression vary regularly in terms of space, and the interbedded-type shale oil is mainly distributed in the lower Qingshankou I Member in the southern Changling Depression. In the north of the Changling Depression or in the upper Qingshankou I Member, the siltstone interlayers become thinner or disappear, and the shale-oil type changes to a pure-shale type (Figure 12).

Table 3. Classification standard of interbedded shale-oil sweet spots of Qingshankou IMember in the Changling Depression.

Parameters	Shale Sweet Spots			Remarks	Siltstone Interlayer Sweet Spots		
	Type I	Type II	Type III		Type I	Type II	Type III
R_o (%)	≥1.2	1.0–1.2	0.7–1.0	Selection zone			
Brittle mineral Content (%)	55–80		<50	Selection zone/layer			
Crude oil density (g/cm^3)	≤0.84	0.84–0.85	0.85–0.87	Selection zone			
Gas-to-oil ratio (m^3/m^3)	≥50	40–50	<40	Selection zone			
Pressure coefficient	≥1.2	1.0–1.2	<1.0	Selection zone			
Monolayer thickness of type I layer (m)	≥8	6–8	<6	Selection zone	2–4	1–3	0–2
TOC (%)	≥2.0	1.2–2.0	<1.2	Selection zone			
Effective porosity (%)	≥4.5	4–4.5	<4	Selection zone	≥11	9–11	<9
Oil Saturation (%)	≥55	50–55	<50	Selection zone/layer	≥55	50–55	<50
OSI (mg/gTOC) for shale or Energy storage coefficient	>100		<100	Selection zone/layer	≥0.18	0.06–0.18	<0.06
Lithofacies	Felsic shale, silty-laminated shale			Selection zone/layer			
Sedimentary Facies	Outer delta front, semi-deep lake, deep lake			Selection zone	Delta front		
Fault system	not developed or has small internal faults		Deep faults developed	Selection zone			

The interbedded-type shale-oil sweet spots are mainly concentrated in the lower Qingshankou I Member (mainly in the Y1–Y3 groups) (Figure 12) in the south of the Changling Depression, with a thickness of around 40–60 m. The pure shale of the Y1 Group is dominated by type II sweet spots of shale oil, and the type I sweet spots were locally developed. The pure shale of the Y2 and Y3 groups developed thick type I sweet spots with a monolayer thickness of 1–3 m and a stable lateral distribution. In the middle and upper parts of the Y1 and Y2 groups, the siltstone interlayers continuously developed, and they mainly corresponded to type I and type II interlayers. In particular, the siltstone interlayer of the Y2 Group was adjacent to the type I pure-shale sweet spots of the Y2 and Y3 groups; therefore, it was the most favorable development interval of the interbedded-type shale oil.

Based on the sweet-spot standard, the optimal exploration area of the interbedded-type shale oil was approximately 639.2 km^2, and this was mainly distributed in the Daqingzi region in the southern Changling Depression. The type I sweet spots of the interbedded-type shale oil is 196.4 km^2 in area, and it is distributed in the H81, H98, and H197 well blocks with the characteristics of "best shale and best siltstone interlayer", in which the shale oil production capacity has achieved breakthroughs. At present, 20 horizontal wells have developed in this type of sweet spot, the initial daily oil production is stable above 6.3 t, and the EUR can be predicted to be 11,500 tons. The type II sweet spots of the interbedded-type shale oil were around 148.2 km^2 and are distributed in the H82, H89, and H87–7 well blocks with the characteristics of "best shale and medium siltstone interlayer".

A total of 15 horizontal wells were developed in this type of sweet spot, and the initial daily oil production was stable at 5.2 t, showing the characteristics of long-term low and stable production.

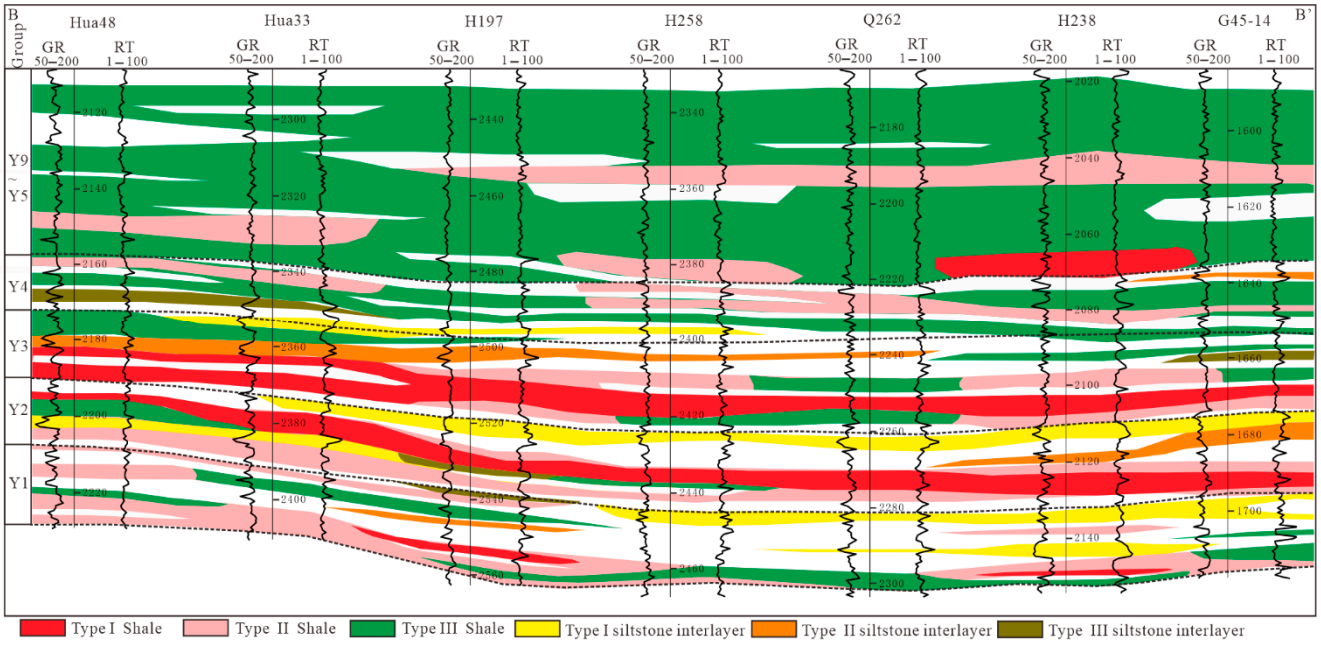

Figure 12. Shale-oil sweet-spot distribution of Qingshankou I Member in Changling Depression (see BB′ in Figure 1 for the profile line).

6. Conclusions

(1) For the Qingshankou shale in the Changling Depression, the siltstone, argillaceous-laminated felsic shale, and the silty-laminated felsic shale have excellent physical properties, mobility, and fracturability, which are the most favorable lithofacies.

(2) The Qingshankou shale in the Changling Depression has a relatively high maturity, and the reservoir space is dominated by intergranular pores, solution pores, intercrystalline pores, and micro-cracks, and there is also a small amount of organic pores. The laminae types control the pore structure and oiliness. Light hydrocarbon components are enriched in the silty laminae and the felsic laminae in a free state.

(3) The high maturity and the interbedded combination of sand and shale ensure the efficient production of the interbedded-type shale oil. Maturity controls crude oil density, the gas-to-oil ratio, and pore pressure. When the R_o > 1.0%, the shale-oil mobility is evidently better. A good combination of sand and shale ensures the sustainable contribution of the pure-shale-oil section.

(4) The interbedded-type shale-oil sweet spots are controlled by the superposition relationship between the siltstone interlayer and the pure-shale sweet spots. The "best shale and best siltstone interlayers" combination is the best, followed by the "best shale and medium siltstone interlayers" combination.

Author Contributions: Conceptualization, L.Y. and D.X.; methodology, W.X. and L.Z.; software, R.W.; validation, L.Z. and J.X.; formal analysis, L.Z.; investigation, R.W. and W.X.; resources, L.Y. and J.X.; data curation, J.X.; writing—original draft preparation, D.X.; writing—review and editing, L.Z.; visualization, R.W.; supervision, L.Y. and D.X.; project administration, L.Y.; funding acquisition, L.Y. and D.X. All authors have read and agreed to the published version of the manuscript.

Funding: This paper was financially supported by the National Natural Science Foundation of China (No. 41972139 and No. 41922015) and the National Science and Technology Major Project of China (Grant No. 2016ZX05061).

Data Availability Statement: The data presented in this study are available on request from the corresponding author.

Conflicts of Interest: The authors declare no conflict of interest.

References

1. Zhao, W.Z.; Hu, S.Y.; Hou, L.H.; Yang, T.; Li, X.; Guo, B.C.; Yang, Z. Types and resource potential of continental shale oil in China and its boundary with tight oil. *Pet. Explor. Dev.* **2020**, *47*, 1–11. [CrossRef]
2. Jin, Z.J. Hydrocarbon accumulation and resources evaluation: Recent advances and current challenges. *Adv. Geo-Energy Res.* **2023**, *8*, 1–4. [CrossRef]
3. Hu, S.Y.; Zhao, W.Z.; Hou, L.H.; Yang, Z.; Zhu, R.K.; Wu, S.T.; Bai, B.; Jin, X. Development potential and technical strategy of continental shale oil in China. *Pet. Explor. Dev.* **2020**, *47*, 877–887. [CrossRef]
4. Sun, J.Y.; Chen, X.W.; Zhang, Y.; Qin, Y.; Chen, C.; Li, W.Z.; Zhou, W.N. Displacement Characteristics of CO_2 to CH_4 in Heterogeneous Surface Slit Pores. *Energy Fuels* **2023**, *37*, 2926–2944. [CrossRef]
5. Li, J.R.; Yang, Z.; Wu, S.T.; Pan, S.Q. Key issues and development direction of petroleum geology research on source rock strata in China. *Adv. Geo-Energy Res.* **2021**, *5*, 121–126. [CrossRef]
6. Wang, X.N.; Li, J.R.; Jiang, W.Q.; Zhang, H.; Feng, Y.L.; Yang, Z. Characteristics, current exploration practices, and prospects of continental shale oil in China. *Adv. Geo-Energy Res.* **2022**, *6*, 454–459. [CrossRef]
7. Fu, J.H.; Guo, W.; Li, S.X.; Liu, X.Y.; Cheng, D.X.; Zhou, X.P. Characteristics and exploration potential of muti-type shale oil in the 7th Member of Yanchang Formation, Ordos Basin. *Nat. Gas Geosci.* **2021**, *32*, 1749–1761.
8. Zhi, D.M.; Tang, Y.; Yang, Z.F.; Guo, X.G.; Zheng, M.L.; Wan, M.; Huang, L.L. Geological characteristics and accumulation mechanism of continental shale oil in Jimusaer Sag, Junggar Basin. *Oil Gas Geol.* **2019**, *40*, 524–534.
9. He, W.Y.; Meng, Q.A.; Feng, Z.H.; Zhang, J.Y.; Wang, R. In-situ accumulation theory and exploration & development practice of Gulong shale oil in Songliao Basin. *Acta Pet. Sin.* **2022**, *43*, 1–14.
10. Sun, L.D.; Liu, H.; He, W.Y.; Li, G.X.; Zhang, S.C.; Zhu, R.K.; Jin, X.; Meng, S.W.; Jiang, H. An analysis of major scientific problems and research paths of Gulong shale oil in Daqing oilfield, NE China. *Pet. Explor. Dev.* **2021**, *48*, 527–540. [CrossRef]
11. He, W.Y.; Meng, Q.A.; Zhang, J.Y. Controlling factors and their classification-evaluation of Gulong shale oil enrichment in Songliao Basin. *Pet. Geol. Oilfield Dev. Daqing* **2021**, *40*, 1–12.
12. Zhang, J.F.; Xu, X.Y.; Bai, J.; Chen, S.; Liu, C.; Li, Y.H. Enrichment and exploration of deep lacustrine shale oil in the first member of Cretaceous Qingshankou Formation, south Songliao Basin, NE China. *Pet. Explor. Dev.* **2020**, *47*, 683–698. [CrossRef]
13. Liu, B.; Sun, J.H.; Zhang, Y.Q.; He, J.L.; Fu, X.F.; Yang, L.; Xing, J.L.; Zhao, X.Q. Reservoir space and enrichment model of shale oil in the first member of Cretaceous Qingshankou Formation in the changling Sag, southern Songliao Basin, NE China. *Pet. Explor. Dev.* **2021**, *48*, 608–624. [CrossRef]
14. Feng, Z.H.; Huo, Q.L.; Wang, X.; Zeng, H.S.; Fu, L. Organic geochemical characteristics and paleosedimentary environments of the source rocks in member 1 of Qingshankou Formation. *Pet. Geol. Oilfield Dev. Daqing* **2015**, *34*, 1–7.
15. Cui, B.W.; Chen, C.R.; Lin, X.D.; Zhao, Y.; Cheng, X.Y.; Zhang, Y.P.; Lu, G.Q. Characteristics and distribution of sweet spots in Gulong shale oil reservoirs of Songliao Basin. *Pet. Geol. Oilfield Dev. Daqing* **2020**, *39*, 45–55.
16. *SY/T 5163-2010*; Analysis Method for Clay Minerals and Ordinary Non-Clay Minerals in Sedimentary Rocks by the X-ray Diffraction. Petroleum Industry Press: Beijing, China, 2010.
17. *GB/T 34533-2017*; General Administration of Quality Supervision, Inspection and Quarantine of the People's Republic of China & Standardization Administration of the People's Republic of China. Measurement of Helium Porosity and Pulse Decay Permeability of Shale. Standards Press of China: Beijing, China, 2017.
18. *GB/T 29171-2012*; General Administration of Quality Supervision, Inspection and Quarantine of the People's Republic of China & Standardization Administration of the People's Republic of China. Rock Capillary Pressure Measurement. Standards Press of China: Beijing, China, 2013.
19. Sheng, P.; Zhang, T.W.; Loucks, R.G.; Shultz, J. Application of mercury injection capillary pressure to mudrocks: Conformance and compression corrections. *Mar. Pet. Geol.* **2017**, *88*, 30–40.
20. Lin, S.H.; Hou, L.H.; Luo, X. Shale Mineralogy Analysis Method, Quantitative Correction of Minerals Using QEMSCAN Based on MAPS Technology. *Appl. Sci.* **2022**, *12*, 5013. [CrossRef]
21. *SY/T 5162-2021*; Analytical Method for Rock Samples by Scanning Electron Microscope. Petroleum Industry Press: Beijing, China, 2021.
22. *SY/T 6490-2014*; Specification for Measurement of Rock NMR Parameter in Laboratory. Petroleum Industry Press: Beijing, China, 2015.
23. Mondal, L.; Singh, K.H. Fluid substitution in NMR T2 distribution and resistivity independent saturation computation using synthetic capillary pressure data. *Pet. Res.* **2023**, *8*, 77–86. [CrossRef]
24. Li, J.B.; Lu, S.F.; Chen, G.H.; Wang, M.; Tian, S.S.; Guo, Z.Q. A new method for measuring shale porosity with low-field nuclear magnetic resonance considering non-fluid signals. *Mar. Pet. Geol.* **2019**, *102*, 535–543. [CrossRef]
25. Liu, B.; Wang, H.L.; Fu, X.F.; Bai, Y.F.; Bai, L.H.; Jia, M.C.; He, B. Lithofacies and depositional setting of a highly prospective lacustrine shale oil succession from the Upper Cretaceous Qingshankou Formation in the Gulong sag, northern Songliao Basin, northeast China. *AAPG Bull.* **2019**, *103*, 405–432. [CrossRef]

26. Liu, S.J.; Cao, Y.C.; Liang, C. Lithologic characteristics and sedimentary environment of fine-grained sedimentary rocks of the Paleogene in Dongying Sag, Bohai Bay Basin. *J. Palaeogeogr.* **2019**, *21*, 479–489.
27. Teng, J.; Liu, B.; Mastalerz, M.; Schieber, J. Origin of organic matter and organic pores in the overmature Ordovician-Silurian Wufeng-Longmaxi Shale of the Sichuan Basin, China. *Int. J. Coal Geol.* **2022**, *253*, 103970. [CrossRef]
28. Lu, Y.B.; Yang, F.; Bai, T.A.; Han, B.; Lu, Y.C.; Gao, H. Shale oil occurrence mechanisms: A comprehensive review of the occurrence state, occurrence space, and movability of shale oil. *Energies* **2022**, *15*, 9485. [CrossRef]
29. Wang, M.; Ma, R.; Li, J.B.; Lu, S.F.; Li, C.M.; Guo, Z.Q.; Li, Z. Occurrence mechanism of lacustrine shale oil in the Paleogene Shahejie Formation of Jiyang Depression, Bohai Bay Basin, China. *Pet. Explor. Dev.* **2019**, *46*, 833–846. [CrossRef]
30. Ren, Q.; Wei, H.; Lei, G.F.; Zhang, W.G.; Ge, B.Y.; Nan, J.X. Effect of microscopic pore throat structure on displacement characteristics of lacustrine low permeability sandstone: A case study of Chang 6 reservoir in Wuqi Oilfield, Ordos Basin. *Geofluids* **2022**, *2022*, 7438074.
31. Zhang, J.Y.; Tao, S.Z.; Wu, S.T.; Liu, G.D.; Zhao, W.Z.; Li, G.H. Controlling effect of pore-throat structures on tight oil accumulation effectiveness in the upper Cretaceous Qingshankou formation, Songliao Basin. *Geoenergy Sci. Eng.* **2023**, *225*, 211689. [CrossRef]
32. Bernard, S.; Horsfield, B.; Schulz, H.M.; Wirth, R.; Schreiber, A.; Sherwood, N. Geochemical evolution of organic-rich shales with increasing maturity: A STXM and TEM study of the Posidonia Shale (Lower Toarcian, northern Germany). *Mar. Pet. Geol.* **2012**, *31*, 70–89. [CrossRef]
33. Gao, Z.Y.; Duan, L.F.; Jiang, Z.X.; Huang, L.L.; Chang, J.Q.; Zheng, G.W.; Wang, Z.W.; An, F.; Wei, W.H. Using laser scanning confocal microscopy combined with saturated oil experiment to investigate the pseudo in-situ occurrence mechanism of light and heavy components of shale oil in sub-micron shale. *J. Pet. Sci. Eng.* **2023**, *220*, 111234. [CrossRef]
34. Krumbein, W.C. The mechanical analysis of fine-grained sediments. *J. Sediment. Res.* **1932**, *2*, 140–149. [CrossRef]
35. Wu, S.T.; Petroleum Geology Committee of China Petroleum Society; Petroleum Geology Committee of China Geological Society. Unconventional Oiland Gas Committee of China Petroleum Society Shale laminar structure and reservoir performance evaluation of Qingshankou Formation in Songliao Basin. In Proceedings of the 6th Symposium on Unconventional Oil and Gas Geological Evaluation and New Energy, Wuhan, China, 9–12 July 2021.
36. Hu, W.F.; Chen, C.; Sun, J.Y.; Zhang, N.; Zhao, J.F.; Liu, Y.; Ling, Z.; Li, W.Z.; Liu, W.G.; Song, Y.C. Three-body aggregation of guest molecules as a key step in methane hydrate nucleation and growth. *Commun. Chem.* **2022**, *5*, 33. [CrossRef]
37. Li, J.B.; Wang, M.; Jiang, C.Q.; Lu, S.F.; Li, Z. Sorption model of lacustrine shale oil: Insights from the contribution of organic matter and clay minerals. *Energy* **2022**, *260*, 125011. [CrossRef]
38. Wang, X.; Wang, M.; Li, J.B.; Shao, H.M.; Deng, Z.X.; Wu, Y. Thermal maturity: The controlling factor of wettability, pore structure, and oil content in the lacustrine Qingshankou shale, Songliao Basin. *J. Pet. Sci. Eng.* **2022**, *215*, 110618. [CrossRef]
39. Liang, C.; Cao, Y.C.; Liu, K.Y.; Jiang, Z.X.; Wu, J.; Hao, F. Diagenetic variation at the lamina scale in lacustrine organic-rich shales: Implications for hydrocarbon migration and accumulation. *Geochim. Cosmochim. Acta* **2018**, *229*, 112–128. [CrossRef]
40. Carlson, R.; Chamberlain, D.E. Steroid biomarker-clay mineral adsorption free energies: Implications to petroleum migration indices. *Org. Geochem.* **1986**, *10*, 163–180. [CrossRef]
41. Slatt, R.M.; O'Brien, N.R. Pore types in the Barnett and Woodford gas shales: Contribution to understanding gas storage and migration pathways in fine-grained rocks. *AAPG Bull.* **2011**, *95*, 2017–2030. [CrossRef]
42. Guo, Y.; Wang, D.P.; Han, X.Y.; Zhang, K.X.; Shang, X.F.; Zhou, S. Evaluation of fracturability of shale reservoirs in the longmaxi formation in southern sichuan basin. *Front. Earth Sci.* **2022**, *10*, 993829. [CrossRef]
43. Zhao, N.; Huang, J.Q.; Li, D.M.; Wu, X.H.; Huang, Q.Z. Sedimentary laws of thin-layer, Fine-grain turbidites of distant-gentle slope: A case from the 1st member of Qingshankou Formation in Dabusu area of west slope, south Songliao basin. *Acta Sedimentol. Sin.* **2013**, *31*, 291–301.
44. Potter, P.E.; Maynard, J.B.; Pryor, W.A. *Sedimentology of Shale*; Springer: New York, NY, USA, 1980; pp. 1–310.
45. Wu, J.; Li, H.; Goodarzi, F.; Min, X.; Cao, W.X.; Huang, L.F.; Pan, Y.Y.; Luo, Q.Y. Geochemistry and depositional environment of the Mesoproterozoic Xiamaling shales, northern North China. *J. Pet. Sci. Eng.* **2022**, *215*, 110730. [CrossRef]
46. Milliken, K.L.; Rudnicki, M.; Awwiller, D.N.; Zhang, T.W. Organic matter–hosted pore system, Marcellus Formation (Devonian), Pennsylvania. *AAPG Bull.* **2013**, *97*, 177–200. [CrossRef]
47. Yan, Q.; Ping, H.W.; Yang, X.; Liu, H.L.; Chen, H.H. Evaluation of Shale Oil Mobility for the Eocene Shahejie Formation in Liutun Sag, Dongpu Depression, Bohai Bay Basin. *Energies* **2023**, *16*, 2101. [CrossRef]
48. Han, Y.J.; Mahlstedt, N.; Horsfield, B. The Barnett Shale: Compositional fractionation associated with intraformational petroleum migration, retention, and expulsion. *AAPG Bull.* **2015**, *99*, 2173–2202. [CrossRef]
49. Chai, Z.H.; Fang, H.W.; Yao, S.M.; Wang, Q. A model for the flocculation-settling-resuspension process of cohesive sediment. *J. Hydraul. Eng.* **2016**, *47*, 1540–1547.
50. Yan, W.; Wang, J.B.; Liu, S.; Wang, K.; Zhou, Y.N. Logging identification for the Longmaxi mud shale reservoir in the Jiaoshiba area, Sichuan Basin. *Nat. Gas Ind.* **2014**, *34*, 30–36.